CrossMark

PAPER

Mapping the hydraulic connection between a coalbed and adjacent aquifer: example of the coal-seam gas resource area, north Galilee Basin, Australia

Zhenjiao Jiang[1,2] · Gregoire Mariethoz[3,4] · Christoph Schrank[2] · Malcolm Cox[2] · Wendy Timms[5]

Abstract Coal-seam gas production requires groundwater extraction from coal-bearing formations to reduce the hydraulic pressure and improve gas recovery. In layered sedimentary basins, the coalbeds are often separated from freshwater aquifers by low-permeability aquitards. However, hydraulic connection between the coalbed and aquifers is possible due to the heterogeneity in the aquitard such as the existence of conductive faults or sandy channel deposits. For coal-seam gas extraction operations, it is desirable to identify areas in a basin where the probability of hydraulic connection between the coalbed and aquifers is low in order to avoid unnecessary loss of groundwater from aquifers and gas production problems. A connection indicator, the groundwater age indictor (GAI), is proposed, to quantify the degree of hydraulic connection. The spatial distribution of GAI can indicate the optimum positions for gas/water extraction in the coalbed. Depressurizing the coalbed at locations with a low GAI would result in little or no interaction with the aquifer when compared to the other positions. The concept of GAI is validated on synthetic cases and is then applied to the north Galilee Basin, Australia, to assess the degree of hydraulic connection between the Aramac Coal Measure and the water-bearing formations in the Great Artesian Basin, which are separated by an aquitard, the Betts Creek Beds. It is found that the GAI is higher in the western part of the basin, indicating a higher risk to depressurization of the coalbed in this region due to the strong hydraulic connection between the coalbed and the overlying aquifer.

Keywords Heterogeneity · Hydraulic connection · Coal seam gas · Groundwater flow · Australia

Introduction

In a sedimentary basin, coal-seam gas (CSG) can be formed by biogenic processes and thermal degradation, and stored in the coal seams by adsorption and dissolution under high pressure. In order to recover the gas, groundwater is extracted from the coalbed to lower the pressure. For example, the Powder River Basin in Montana, USA, is a major CSG producing area, and approximately 2.5×10^5 m^3/d of groundwater is co-produced from around 25,000 wells (Morin 2005; Myers 2009). In the Bowen and Surat Basins, which are major CSG production areas in eastern Queensland, Australia, early estimates in 2008 indicated that approximately 2.0×10^5 m^3/d of groundwater was pumped to recover CSG and the volume of groundwater extraction for CSG production continued to increase (Helmuth 2008).

The northern Galilee Basin (GB) in central Queensland is considered as a potential target for CSG production. The coal-bearing formations within the GB underlie the aquifers in the Great Artesian Basin (GAB), which is one of the most important groundwater reservoirs in Australia (Habermehl 2006). The GB coalbeds and GAB aquifers are separated by

✉ Zhenjiao Jiang
jiangzhenjiao@hotmail.com

1 Key Laboratory of Groundwater Resources and Environment, Ministry of Education, College of Environment and Resources, Jilin University, Changchun 130021, China

2 School of Earth, Environmental & Biological Sciences, Queensland University of Technology, Brisbane, QLD 4001, Australia

3 Institute of Earth Surface Dynamics, University of Lausanne, 1015 Lausanne, Switzerland

4 School of Civil and Environmental Engineering, University of New South Wales, Sydney, NSW 2052, Australia

5 School of Mining Engineering, University of New South Wales, Sydney, NSW 2052, Australia

Springer

aquitards. However, leakage through a heterogeneous aquitard could possibly lead to significant groundwater loss from the GAB aquifers and result in inadequate depressurization of the coalbed, thus inhibiting gas recovery (Beckers and Cook 2013; Hamawand et al. 2013). Therefore, it is critical to assess the potential of hydraulic connection between the GB coalbeds and the GAB aquifers due to leakage via the separating aquitard.

Leakage may occur at the local scale through the drillhole or through conductive fractures and faults in the aquitard. At the regional scale, a complex sedimentary environment may have produced conductive networks in heterogeneous aquitards such as the interconnected sandstone channel depositions created in fossil river systems (De Marsily et al. 2005; Koltermann and Gorelick 1996). The occurrence of local-scale leakage is often investigated by tracers such as strontium and carbon isotopes (e.g. Frost et al. 2002; Sharma and Frost 2008), while leakage at regional scale is often tested by numerical modeling of groundwater flow processes (e.g. Anna 2003; Birkholzer et al. 2009; Gasda 2010; Zhang et al. 2009). In the GB the localized leakage of gas and water between the coal-bearing formations and the GAB aquifers was identified based on dissolved methane (Moya et al. 2015). This current study focuses on the evaluation of hydraulic connection between a coalbed and an aquifer attributed to regional-scale leakage.

To this end, numerical modeling could be an effective approach (e.g. Cao et al. 2013; Giambastiani et al. 2012; Storey et al. 2003; Winter 1999); however, one difficulty is that it requires the conceptualization of the geometry of water-bearing formations, the heterogeneous hydraulic parameters in multiple water-bearing formations, the boundary conditions, and the recharge and discharge of the groundwater system. Moreover, the effects of the conceptualization need to be verified against the observations of variables such as water levels and groundwater discharge (Harbaugh et al. 2000). In the multilayered aquifer-aquitard systems of the GB and GAB, it is difficult to adequately conceptualize hydrogeology conditions as there is a lack of hydrogeology data.

Another approach is to start from the observation that the hydraulic connection between coalbed and the aquifer is mainly determined by the properties of their separating aquitard, including aquitard thickness, lithology, lithology sequence and the permeability of each lithoface unit. The influences of these properties on the subsurface flow and transport can be quantified by the connectivity indicators (e.g. Dell'Arciprete et al. 2014; Michaelides and Chappell 2009; Oriani and Renard 2014; Zinn and Harvey 2003). Several connectivity indicators were proposed in the literature which fall into two broad categories: (1) static connectivity indicators which depend on the connectivity structure of the parameter fields; and (2) dynamic connectivity indicators which refer to the physical processes such as flow and transport in heterogeneous subsurface media (Renard and Allard 2013).

Commonly used static indicators include statistical indicators, which are inferred from two-point or multiple-point correlation of hydraulic conductivity (Knudby and Carrera 2005; Michaelides and Chappell 2009). Typical dynamic connectivity indicators include flow connectivity, which is the ratio between effective hydraulic conductivity and the geometric mean of local hydraulic conductivity, and solute transport connectivity, which is defined as the ratio between average arrival time and the arrival time of a smaller fraction of tracers (Bianchi et al. 2011; Knudby and Carrera 2005, 2006). Although the dynamic connectivity indicators are defined based on forward numerical modeling, the model domain focuses on a single target formation (here the aquitard separating the aquifer and coalbed) and the boundary conditions do not necessarily follow the real field conditions. Arbitrary constant head boundaries are often used, as long as they allow water flow or solute transport through the target formation (Bianchi et al. 2011; Knudby and Carrera 2005).

The aforementioned connectivity indictors succeed in representing the intrinsic properties of geological formations (Bianchi et al. 2011; Dell'Arciprete et al. 2014); however, as far as the authors are aware, they have not been used to infer the degree of hydraulic connection between two aquifers separated by an aquitard at the basin scale. Following the logic of deriving the transport connectivity indicator, a groundwater age indicator (GAI) is proposed here, to estimate the hydraulic connection between two aquifers. GAI is a dynamic indicator which (1) considers both vertical flow and lateral flow components in the aquitard; (2) defines the mixing processes of the newly recharged water and the existing water in the aquitard; (3) is time-independent but considers the transient flow/transport processes in the aquitard.

The GAI was validated by synthetic case studies and was then applied in the GB, Australia. The GAI statistics (variance and mean) in space were mapped to represent the degree of hydraulic connection between the coalbed and the aquifer, which can suggest optimum locations for the gas/water production wells.

Materials

Geological setting

The GB in central Queensland (Fig. 1a) is a large intracratonic basin filled with Late Carboniferous to Middle Triassic sedimentary rocks. Based on the depositional environments, the sedimentary formations in the GB are divided into two major successions: the Joe Joe Group and the Betts Creek Beds and related formations (Fig. 1b; Evans 1980). The Joe Joe Group was deposited during the Early Permian and is composed of fluvial and lacustrine sediments interbedded with glaciogenic and volcano-lithic beds. From the late Early Permian period,

Fig. 1 a Location map of the Galilee Basin, in Queensland (*QLD*), Australia, **b** the stratigraphy within the north Galilee Basin, **c** location of lithology logs and hydraulic conductivity tests. The data for lithology logs and drill stem tests are extracted from the well completion reports of the Department of Natural Resources and Mines (Evans 1980)
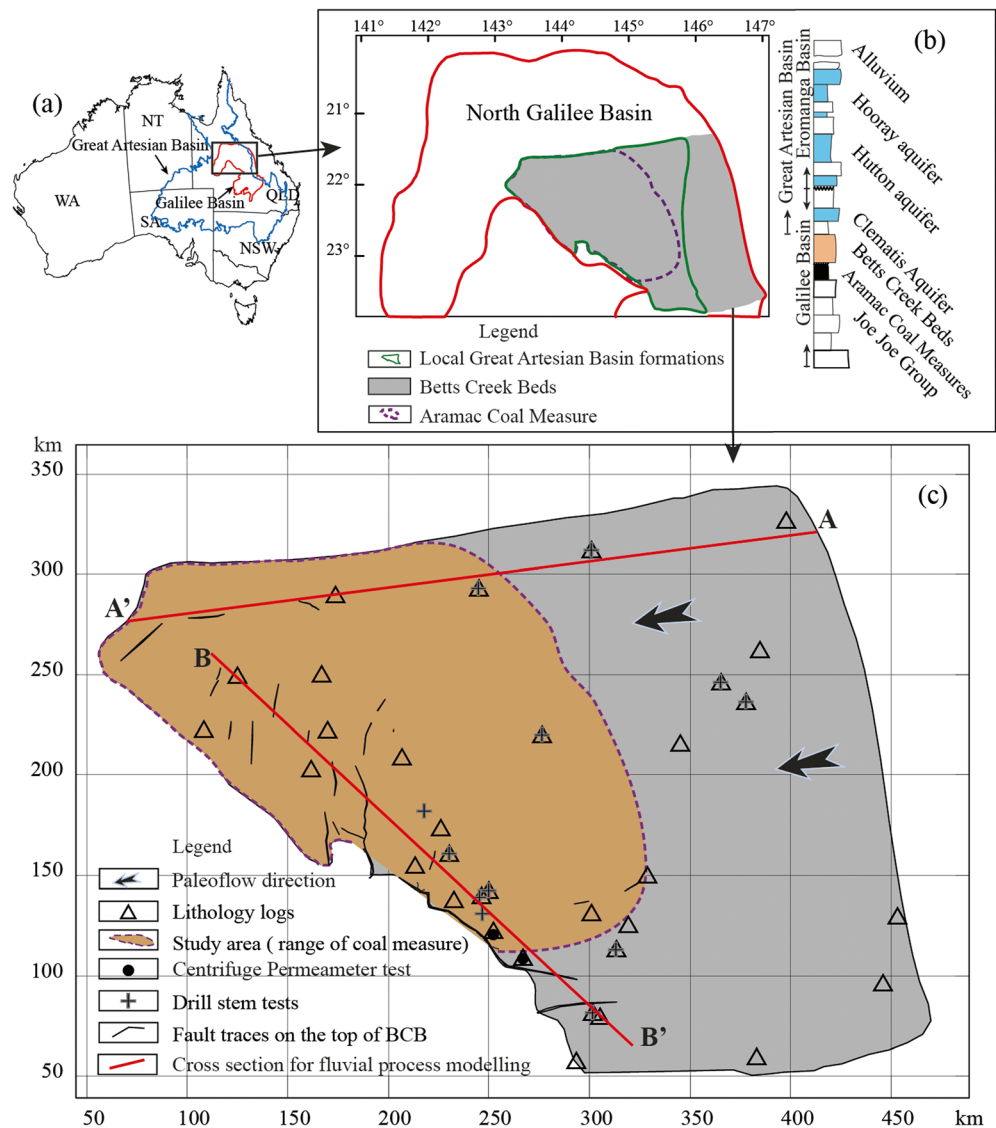
the development of widespread peat swamps resulted in the deposition of the Aramac Coal Measures overlying the Joe Joe Group (Hawkins and Green 1993); however, tectonic uplift at the end of the Early Permian resulted in a partial erosion of the Aramaic Coal Measures and formed an unconformity upon which sediments of the second succession were deposited.

The second succession is composed of the Betts Creek Beds (BCB), Rewan Formation, Clematis Sandstones and Moolayember Formation (Fig. 1b). These sediments were largely deposited by westerly or south-westerly flowing rivers during the Late Permian to Middle Triassic (Allen and Fielding 2007). Following this depositional period, an east–west contractional episode in the Late Triassic resulted in uplifting, folding and partial erosion of the Moolayember Formation prior to depositing the sediments of the Eromanga Basin (Hawkins and Green 1993), which is a sub-basin of the GAB (Fig. 1b).

The Aramac Coal Measures underlying the GAB have been explored as a potential source of coal seam gas (CSG) production. Extraction of CSG/water from this coalbed could possibly induce groundwater loss from the GAB water-bearing formations due to the leakage via the BCB. This study addresses part of the north GB (Fig. 1b,c), and quantifies the hydraulic connection between the Aramac Coal Measures and the GAB aquifer attributed to the leakage via the BCB.

BCB heterogeneity

As the leakage ability of the BCB depends on the spatial distribution of the hydraulic parameters, it is important to characterize the heterogeneity of the BCB before quantifying the degree of hydraulic connection between the coalbed and the overlying aquifer. The hydraulic conductivity (*K*), specific storage (S_s) and thickness (*h*) of BCB have been estimated by

stochastic fluvial process modeling (SFPM) and sequential Gaussian simulation (Jiang et al. 2015; 2016), where the semivariograms in the directions perpendicular and parallel to the paleoflow were inferred separately. Although this way of proceeding is slightly unusual in geostatistics, it is used here as a very practical solution to address the lack of lithology logs. The methodology is briefly summarized as follows:

There are 16 lithology logs in the direction perpendicular to the paleoflow, in the neighborhood of line B–B′ (Fig. 1). All of these logs record the elevations of both the top and bottom of the BCB, but only ten of them continually record the lithology components at different depth. This results in a fairly large number of data pairs for BCB thickness, and thus the semivariograms of thickness in this direction can be evaluated (Fig. 2a; Jiang et al. 2016). The modeled semivariogram of the BCB thickness follows a Gaussian model with the range of around 90 km and the sill of 3,300 m^2. The value of the sill is comparable to the variance of 16 measured thicknesses (3,359 m^2); however, the semivariogram of the sandstone

proportion over the total thickness (P_s) in this direction cannot be directly inferred from the limited number of logs.

The number of data pairs in the direction of the paleoflow (line A–A′ on Fig. 1) are not sufficient to compute a semivariogram. SFPM was thus employed to reproduce the sedimentary processes, which yielded the thickness and P_s of the BCB at 1,000 positions (Jiang et al. 2016). These results were validated by four sets of lithology logs surrounding line A–A′, and were then used to infer the semivariograms of thickness and P_s in the direction of the paleoflow (Fig. 2b,c). As a result, the modeled semivariogram of the BCB thickness can now be fitted by a Gaussian model with a range of 120 km and a sill of 5,200 m^2, and the semivariogram of P_s at the lags less than 30 km is fitted using an exponential model with a range of 20 km and a sill of 0.062.

Based on the ranges of thickness semivariograms in different directions, the anisotropy factor of the semivariograms in the directions perpendicular and parallel to the paleoflow is estimated as 0.75 (90 km/120 km). Subsequently, the range of

Fig. 2 Experimental and modeled semivariograms of thickness on line B–B′ (a) and on line A–A′ (b), and the semivariogram of sandstone proportion on line A–A′ (c) (Jiang et al. 2016)
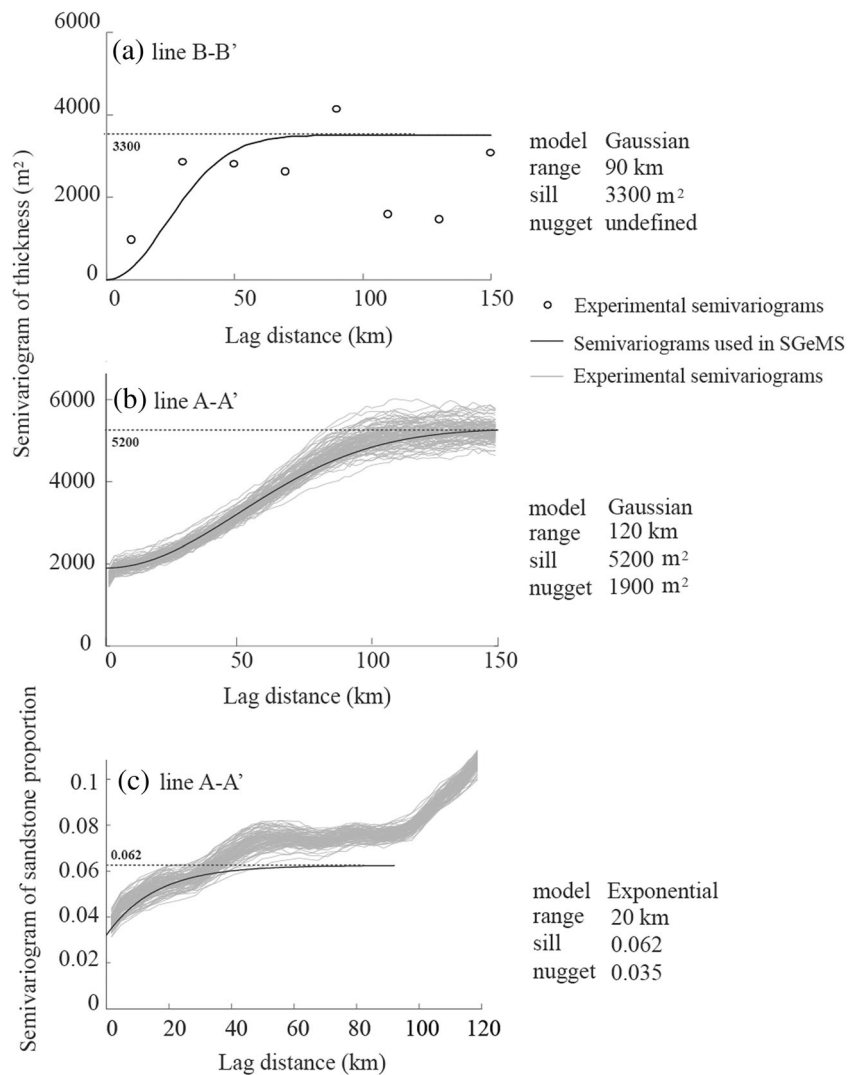
P_s semivariogram along line B–B′ is estimated as 15 km (Jiang et al. 2016). It is observed in Fig. 2a,b that the semivariogram in the direction of paleoflow has a higher range and sill, which means the stronger correlation and variation of the thicknesses in the direction of paleoflow than that perpendicular to the paleoflow. The anisotropy aligned with the paleoflow direction makes is a logic geological interpretation. The data in Fig. 2a,b indicate that the anisotropy very likely relates to the known direction of paleoflow, rather than the non-uniformly distributed data sets.

According to the semivariogram models described in the preceding, sequential Gaussian simulation in the SGeMS geostatistical package (Remy et al. 2009) was employed to generate random spatial distributions of thickness and P_s, conditionally to 32 lithology logs (Fig. 1c). Ten realizations were generated, and the mean and variance of these realizations are illustrated in Fig. 3.

The P_s can be converted to an upscaled hydraulic conductivity and specific storage using a classical averaging method (Freeze and Cherry 1977):

$$K_h(\mathbf{x}) = K_s P_s(\mathbf{x}) + K_c[1 - P_s(\mathbf{x})] \quad (1)$$

$$K_v(\mathbf{x}) = \frac{1}{P_s(\mathbf{x})/K_s + [1 - P_s(\mathbf{x})]/K_c} \quad (2)$$

$$S_s(\mathbf{x}) = P_s(\mathbf{x})\rho g(\alpha_s + n_s\beta) + [1 - P_s(\mathbf{x})]\rho g(\alpha_c + n_c\beta) \quad (3)$$

where K_h is the horizontal hydraulic conductivity (m/d), K_v the vertical hydraulic conductivity (m/d), K_s the hydraulic conductivity of the sandstone (m/d), K_c the hydraulic conductivity of siltstone (m/d), S_s the specific storage (m^{-1}), P_s the sandstone proportion, α_s the compressibility for sandstone

$(2.0 \times 10^{-10} \text{ Pa}^{-1})$ and α_c the compressibility for siltstone $(1.5 \times 10^{-10} \text{ Pa}^{-1}$; Horne 1995), β the compressibility of water $(4.6 \times 10^{-10} \text{ Pa}^{-1})$, g the gravitational acceleration coefficient $(9.8 \text{ m}^2/\text{d})$. n_s is the porosity of sandstone (0.2), and n_c is the porosity of siltstone (0.25), the values of which are estimated by the lithological and geophysical logs in the Betts Creek Beds (Evans 1980).

A total of 37 drill stem tests (DST) were conducted in 11 drillholes, which enabled estimation of the hydraulic conductivity. To evaluate K_s, the hydraulic conductivity values measured by 12 DST that were conducted only within sandstone were selected. These DST provide the horizontal K_s in the test intervals. Due to the variability of grain size and porosity in sandstones, K_s varies from 0.01 to 0.1 m/d with an average value of 0.038 m/d. As the test intervals are relatively small (less than 1 m) and K_s will be upscaled to the K values at the numerical scale, the difference between vertical and horizontal K_s at centimeter-scale is neglected.

However, the direct measurement of K_c in the field is difficult, as an unrealistic testing time or hydraulic pressure gradient is required to allow water flow through rocks that have an extremely low hydraulic conductivity. To address this, three 30-mm rock core samples (siltstone, claystone and shale) were collected from drillholes penetrating in the BCB, and K_c was tested by use of a centrifuge permeameter. This approach allows for large hydraulic pressure differences between the top and bottom of the test sample, and accounts for the influences of fluid chemistry and formation stresses (Timms et al. 2014). After 50–70-h tests, K_c for three rock samples stabilized at values varying between 10^{-6} and 10^{-7} m/d (Fig. 4).
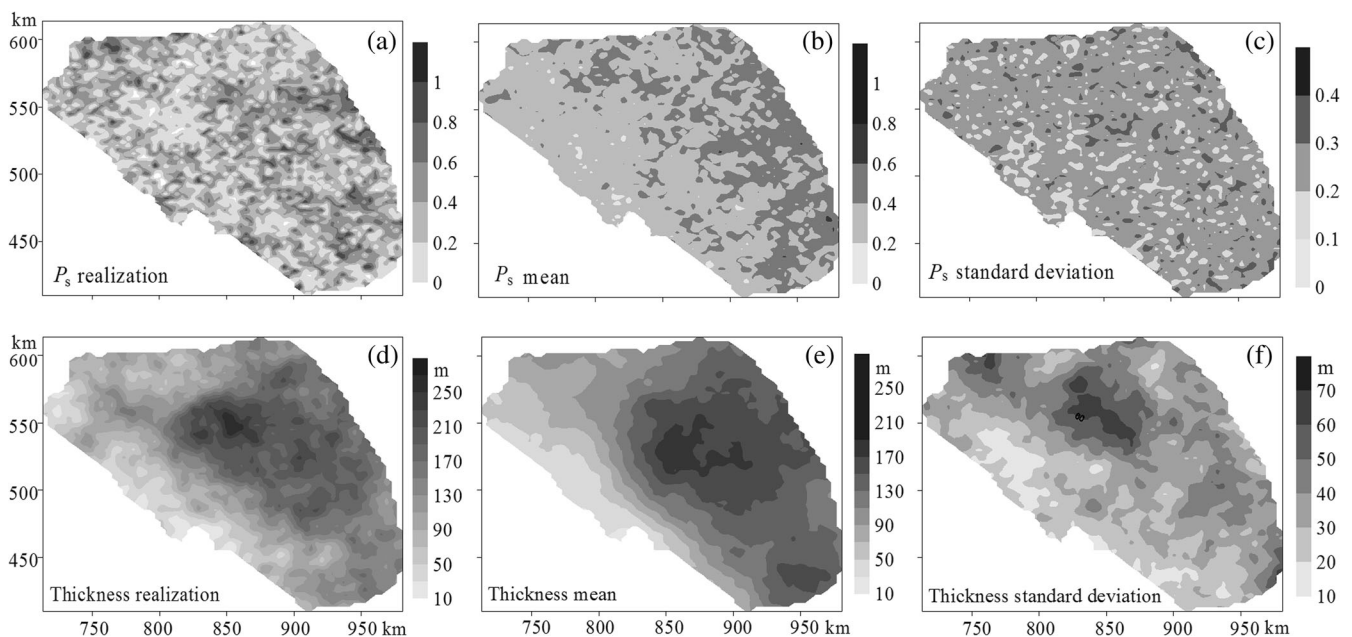
Fig. 3 **a–c** Sandstone proportion (P_s) relative to the entire thickness and **d–f** thickness of Betts Creek Beds created by the stochastic fluvial processes model and sequential Gaussian simulation. The mean and standard deviation are calibrated based on 10 realizations from sequential Gaussian simulation
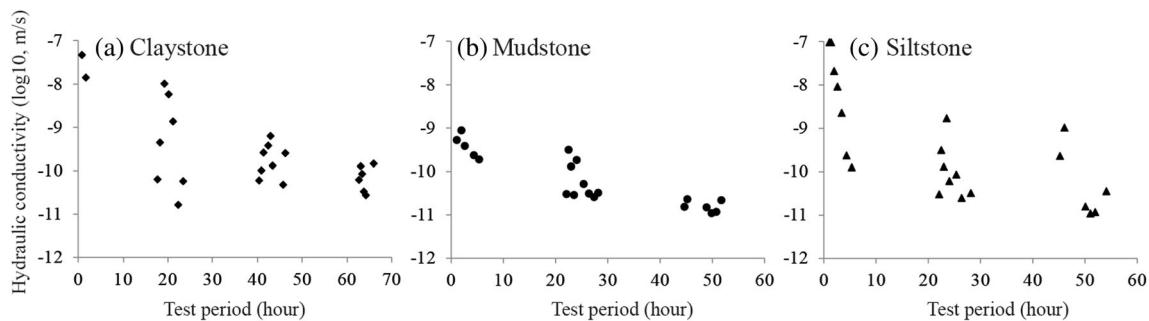
Fig. 4 Hydraulic conductivity measured by a centrifuge permeameter test according to inflow water volume for **a** claystone, **b** mudstone, and **c** siltstone. The values stabilize at $10^{-10.5}$–$10^{-11.5}$ m/s (approximately 10^{-6}–10^{-7} m/d) after about 60 h

## Hydraulic connection indicator

Concept

The hydraulic connection between the coalbed and overlying aquifer is determined by the properties of the separating aquitard including parameters such as the aquitard thickness, the spatial distribution of K_h and K_z. It is necessary to develop an indicator to quantitatively bridge these multiple properties in the aquitard to the degree of hydraulic connection between aquifers. A connection indicator is proposed based on the groundwater age modeling.

Before deriving the connection indictor, the pattern of outflow groundwater age via an arbitrary synthetic aquitard was calibrated in FEFLOW 6.2 (Diersch 2002) . A relatively small aquitard with the size of 7.0 m × 7.0 m × 1.5 m (along x, y, z directions, respectively) is constructed to save the computational time (Fig. 5a). The heterogeneous hydraulic conductivity in the aquitard is generated by sequential Gaussian simulation in SGeMS on the grid with a resolution of 0.1 m in both length and height (Fig. 5a). Parameters of the semivariograms used to generate this synthetic aquitard are summarized in Table 1. The specific storage is assumed to be 0.0001 m^{-1}. A constant age boundary of zero is evenly assigned on the top. The synthetic aquitard is surrounded by no flow boundaries. Both the top and bottom of the aquitard are defined as the constant-head boundaries, with the water levels of 10 and

9.8 m, respectively. Driven by the hydraulic gradient, groundwater flow from the top to the bottom of the aquitard; the groundwater age is observed at 49 positions evenly at the bottom.

The governing equations for groundwater flow and age are solved using a finite element scheme. The model domain is discretized as 15 × 223,320 triangle prism elements. The spatial resolution on both the horizontal and vertical direction is around 0.1 m; however, the heterogeneous hydraulic conductivities in Fig. 5a are estimated at the cubic element at a resolution of 0.1 m. A nearest neighbor interpolation is used in FEFLOW to convert the hydraulic conductivities output from SGeMS to the grid in FEFLOW. The implicit time integration is employed. The magnitudes of time step (here from 0.1 to 20 d) are internally calculated in FELOW following the second-order AB scheme (forward Adams-Bash forth/ backward trapezoid scheme) to assure the solution convergence (Diersch 2002; Kolditz et al. 1998).

The simulated results are illustrated in Fig. 5b. As shown, in the first day, the outflow ages at 49 positions are equal to the simulation time, because the newly recharged water from the top has not reached the bottom and the outflow water is entirely coming from the existing water in the synthetic aquitard. After that, the outflow age becomes lower than the simulation time due to the mixing of the newly recharged water from the top of the formation and the existing water in the aquitard. When the outflow entirely comes from the newly
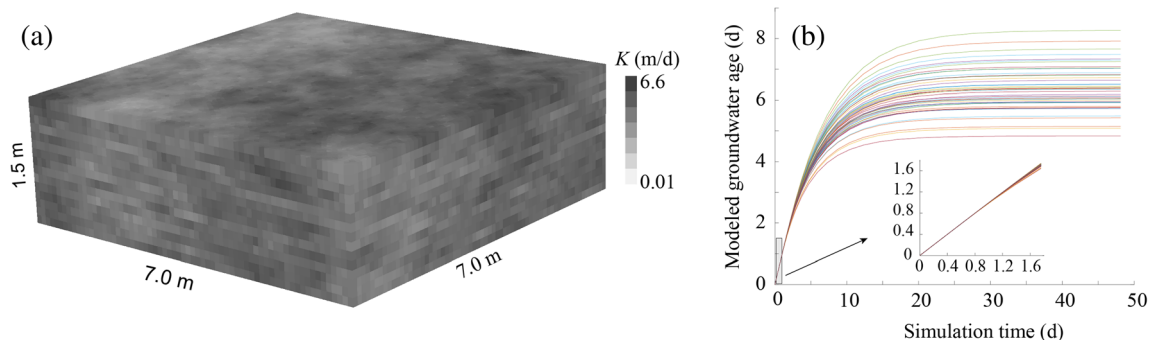
Fig. 5 **a** The synthetic geological model generated by sequential Gaussian simulation in SGeMS, and **b** the modeled groundwater ages at 49 positions on the bottom of the model showing an increase with the simulation time and then stablizing

Table 1 The parameters of semivariogram to create the synthetic aquitard

Directions	Range	Sill	Nugget
x	5	0.2	0.01
y	4	0.2	0.01
z	1	0.2	0.01

recharged water, the outflow age approaches a constant value. The stabilized age observed at each position at the bottom represents the average travel time from the formation top to this position.

The pattern of outflow groundwater age in Fig. 5b can be mathematically expressed as:

$$A(\mathbf{x}, t) = F_e(\mathbf{x}, t)t + [1 - F_e(\mathbf{x}, t)]t_0(\mathbf{x}) \qquad (4)$$

where $\mathbf{x}$ is the coordinates at the aquitard bottom, A is the outflow age, F_e is the fraction of the existing groundwater in the outflow, $1 - F_e$ represents the fraction of newly recharged groundwater, t is the simulation time, and t_0 is the effective time water needs to reach the bottom, which is defined as:

$$t_0(\mathbf{x}) = \frac{1}{q_T(\mathbf{x})} \int_0^\infty t(q, \mathbf{x}) dq \qquad (5)$$

where q_T is the outflow rate from a specific bottom area (m^3/d) sourcing from the newly recharged water, with q of q_T having a travel time $t(q)$.

It is simply assumed that F_e decreases from 1.0 to 0 following a linear process, which is

$$F_e(\mathbf{x}, t) = 1 - b(\mathbf{x})t \qquad (6)$$

where b is the decreasing rate of existing groundwater in the outflow.

Substituting Eq. (6) into Eq. (4) and differentiating with respect to t results in:

$$\frac{dA(\mathbf{x}, t)}{dt} = 1 - 2b(\mathbf{x}) \cdot t + b(\mathbf{x}) \cdot t_0(\mathbf{x}) \qquad (7)$$

Solving Eq. (7) subject to

$$\frac{dA(\mathbf{x}, t)}{dt} = 0 \qquad (8)$$

leads to the appearance time (t_p) of the peak groundwater age as a function of both b and t_0:

$$t_p(\mathbf{x}) = \frac{t_0(\mathbf{x})}{2} + \frac{1}{2b(\mathbf{x})} \qquad (9)$$

Equation (9) is based on a linear assumption for F_e (Eq. 6). Similarly, a relationship can also be obtained between t_p, t_0 and b for different formulations of F_e such as $t_p = t_0 + 1/b$ with respect to $F_e = e^{-bt}$.

In general,

$$t_p(x) = f[t_0(x), b(x)] \qquad (10)$$

At an arbitrary position, a larger t_p corresponds to a larger t_0 and a smaller b. A larger t_0 value means that groundwater takes a longer time to penetrate the aquitard, meaning that the average groundwater flow velocity (v) is low from the top of the aquitard to the selected position at the bottom. A smaller b value indicates that the fraction of old groundwater in the outflow takes a longer time to decrease to zero, suggesting less flow from the formation top to the selected position at the bottom. In other words, by releasing the particles evenly at the top of the aquitard, it is expected to collect a smaller amount of particles at the position with higher t_p on the bottom, while taking a longer time. This suggests a weaker connection between the position with the higher t_p and the top of the aquitard when compared to the other positions. Therefore, t_p can indicate the degree of hydraulic connection between the water-bearing formations separated by the aquitard.

For convenience, a novel connection indicator is defined as:

$$\text{GAI}(\mathbf{x}) = \log_{10}\left[\frac{\bar{t}}{t_p(\mathbf{x})}\right] \qquad (11)$$

where GAI represents the groundwater age indicator, $\bar{t}$ is spatially averaged value of t_p calculated at the entire bottom of the aquitard. The degree of connection is therefore positively related to the GAI value. The position with a smaller GAI (larger t_p) is suitable to site the gas/well in the coalbed, because depressurization at this location will have a weak influence on the adjacent aquifer, due to the weak hydraulic connection between this position and the adjacent aquifer.

Validation with the synthetic aquitard

Using Fig. 5b and Eq. (11), the distribution of GAI at the bottom of the synthetic aquitard is evaluated (Fig. 6b). The spatial distribution of GAI is compared to the distribution of the vertical hydraulic conductivity of the aquitard (K_z). It is observed that the pattern of GAI is similar to K_z (Fig. 6a,b), suggesting the significant control of K_z on the connection between the water-bearing formations overlying and underlying the aquitard. However, GAI is smoother in space than the distribution of K_z, because GAI considers both lateral and vertical flow in the aquitard. This advantage of GAI in contrast to the K_z is further demonstrated in section 'Benchmark test'.

Furthermore, three positions were selected corresponding to the minimum (W3), median (W2) and maximum (W1) GAI, respectively, to locate the depressurization position at the bottom of the aquitard (Fig. 6b). The initial water level in the entire aquitard is assigned as 10 m. Induced by 0.2 m

Fig. 6 **a** The spatial distribution of the vertical hydraulic conductivity (K_z) of the synthetic aquitard, and **b** groundwater-age-indicator distribution at the aquitard bottom, and three wells selected based on the positions with minimum (*W3*), median (*W2*) and maximum (*W1*) groundwater age indicator (*GAI*) to validate the groundwater age indictor
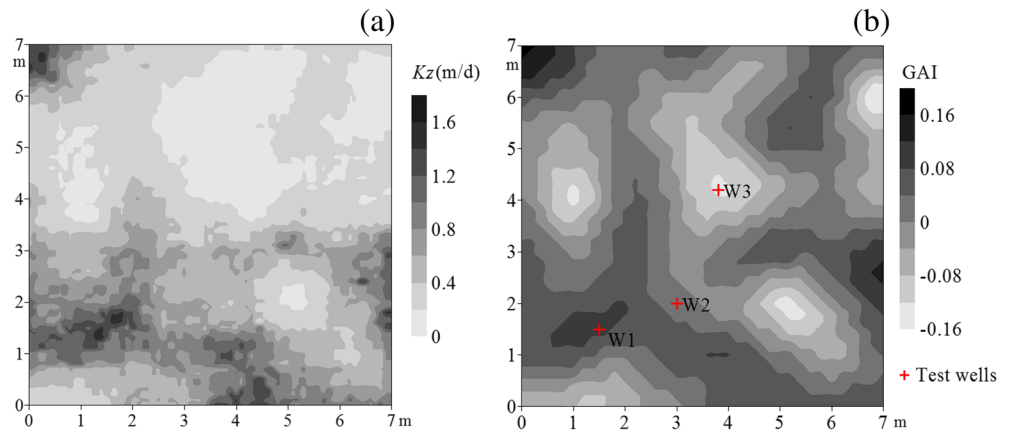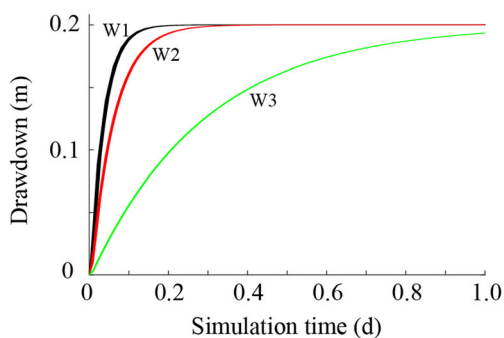

drawdown at W1, W2 and W3, respectively, the water-level responses are observed at 49 positions evenly located on the top of the aquitard. This setting is an analog to the CSG extraction, where the coal bed underlying the aquitard is depressurized and the water-level responses in the adjacent aquifer overlying the aquitard are investigated.

As shown in Fig. 7, the simulated water levels at all 49 positions are almost identical, because the hydraulic conductivity in this synthetic aquitard is sufficiently large to allow the water responses to spread rapidly in the aquitard before affecting the top of the aquitard. However, depressurization at W1 induces a fast drawdown on the formation top in the first 0.1 day and then stabilizes at 0.2 m. The same drawdown at W3 induces a slow decrease of water level at the top. More water losses are induced by the pumping at W1; therefore, the depressurization well located at W1 can impact the water resources more strongly than W2 and W3, which confirms that GAI can help define the optimal locations for gas/water extraction in the coalbed, and that the position with lower GAI is more suitable for depressurization.

Benchmark test

The performance of GAI for a low-permeability aquitard with a tilted permeable channel was then examined (Fig. 8a). In

Fig. 7 The water-level drawdowns at 49 positions at the formation top, which are induced by a water-level drawdown (0.2 m) at locations *W1*, *W2* and *W3*, respectively
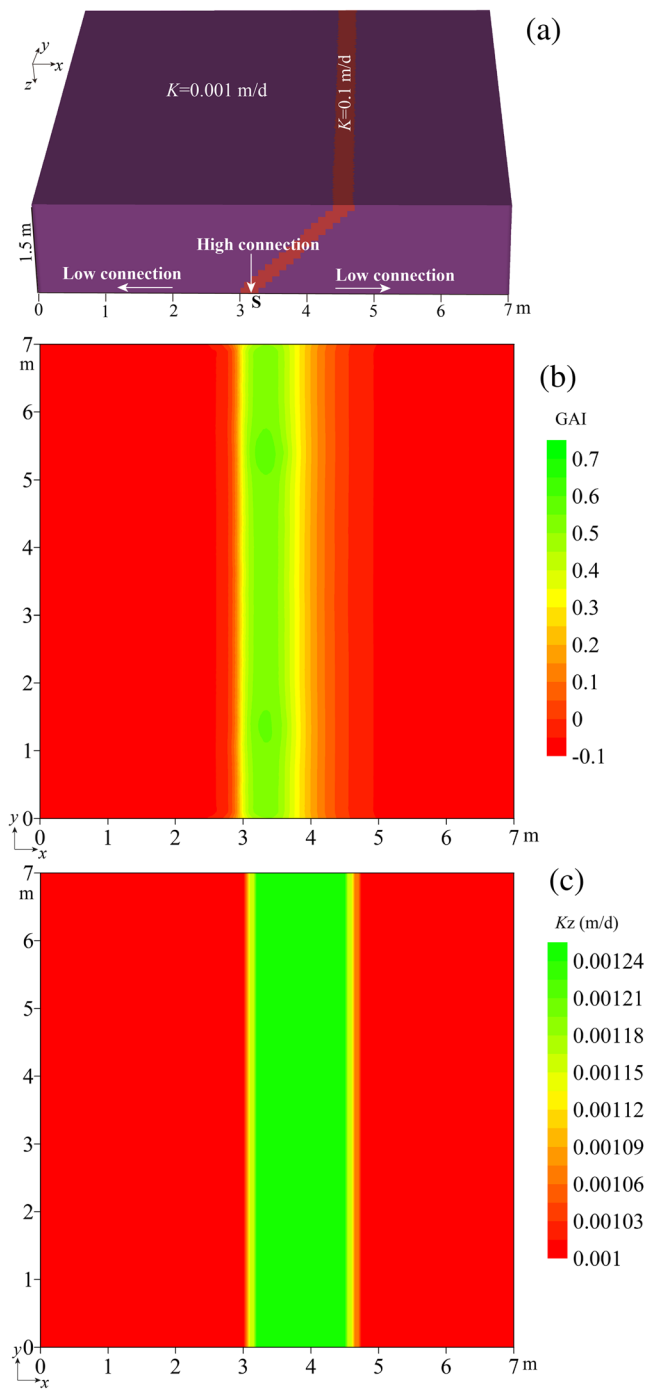
such a model, it is accepted that the middle part on the aquitard bottom (position S in Fig. 8a) is well connected to the aquitard top, due to the short-circuit via the conductive channel. The degree of hydraulic connection reduces towards both sides. According to this phenomenon, the benchmark test is conducted as follows: the permeability of the aquitard is set to 0.001 m/d, while the permeability of the channel is set to 0.1 m/d and constant heads of 10 and 9.8 m are assigned on the top and bottom of the aquitard, to allow a downward flow via the aquitard. Groundwater age on the model top is zero, which indicates the newly recharged water. Groundwater age is observed at the bottom of the model and then converted to values of GAI according to Eq. (11).

The resulting spatial distribution of GAI is illustrated in Fig. 8b. The high GAI in the middle suggests strong hydraulic connection between the top and bottom of the aquitard, which is explained by the depressurization at this position in the aquifer underlying the aquitard which has a large influence on the opposite water bearing formations. The values of GAI decrease towards both sides, following the common sense of hydraulic connection shown in Fig. 8a. In contrast, when soley considering averaged hydraulic conductivity, it is only possible to identify an area of uniformly connected strata (Fig. 8c).

This test shows that GAI is a reliable indicator to represent the degree of hydraulic connection between the aquifers underlying and overlying an aquitard, performing better than the vertical hydraulic diffusivity (here the vertical hydraulic conductivity assuming a constant specific storage).

The sensitivity of GAI to the boundary conditions used on the top and bottom of the formation is analyzed in Fig. 9, where the constant head of 10 m is fixed on the aquitard top, and the water head on the bottom is fixed at values of 2, 7 and 9.8 m. Each model is run for 200 days, which allows the groundwater age to stabilize in space. As shown in Fig. 9a,b,c, the variation of hydraulic gradient can induce the variation in groundwater age. The groundwater age decreases with increased gradient, due to the speed-up of groundwater flow from the top to bottom; however, the pattern of GAI in

Fig. 8 **a** A synthetic aquitard with binary hydraulic conductivity. The spatial distribution of **b** GAI values and **c** the vertical hydraulic conductivity (K_z) averaged over the entire thickness of the aquitard

can be applied at the regional scale as the flow processes in the aquitard and the groundwater age evolution at different scales follow the same governing equations.

Application to the Galilee Basin (GB)

In order to evaluate the connection between the Aramac Coal Measures and the GAB aquifers separated by the BCB, the GAI distribution at the bottom of the BCB is estimated based on the transient groundwater flow and age modeling in FEFLOW. The area of the model domain is 35,075 km^2, which corresponds to the range of the Aramac Coal Measures in the study area (Fig. 1c). The BCB is divided into 15 layers (Fig. 10b). The FEFLOW grid contains 34,450 cells in each layer with a length scale of 500–1,000 m horizontally and 1–30 m vertically. The maximum thickness of the BCB is about 260 m.

The groundwater age is modeled to infer the hydraulic connection between the coalbed and overlying aquifer, rather than to indicate the real groundwater age in the basin. It is not necessary to define the boundary conditions for the BCB following the real situation in the GB. Instead, the boundary conditions are assigned following the logic described in section 'Concept'. The constant heads of 500 and 300 m are assigned at both the top and bottom of the BCB, respectively, with two considerations: (1) a large hydraulic gradient between the top and bottom of the BCB is used to allow groundwater to penetrate the aquitard in a relatively short time, (2) the constant heads at the top and bottom are larger than the thickness of the aquitard to assure the confined condition during the simulation. These boundary conditions create a downward flow with diversion related to the heterogeneity of the BCB. No-flow boundary conditions are imposed on the lateral faces of the BCB. As the lateral extent of BCB is sufficiently large, the influence of no-flow lateral boundaries on the downward flow process is negligible. A similar assumption is used and tested in Bianchi et al (2011). A constant age of zero is evenly assigned at the top of the BCB, and the groundwater age is observed at the BCB bottom. A simulation period of 3,000 days is employed to assure the appearance of peak groundwater age. The GAI can then be calculated according to the groundwater age evolution at the BCB bottom using Eq. (11).

The thickness and hydraulic parameters of the BCB are inferred in section 'BCB Heterogeneity'. However, the results are subject to uncertainties, namely (1) the modeling uncertainties, including the uncertainties in evaluating the BCB thickness, sandstone proportion and lithology sequence, and (2) measurement uncertainties due to the limited number of K_s and K_c measurements. The impact of these uncertainties on the spatial distribution of GAI are examined as follows:

three cases does not vary significantly with different boundary conditions (Fig. 9d,e,f).

Both preceding tests suggest that the GAI is a reliable and robust indictor for mapping the hydraulic connection between two water-bearing formations separated by a heterogeneous aquitard. Although the GAI is derived and validated according to the results of a synthetic case at a relatively small scale, it

Fig. 9 **a**–**c** Cross-sectional view of groundwater age distribution and **d**–**f** the spatial distribution of the GAI at the bottom of the synthetic formation

Groundwater age (day)
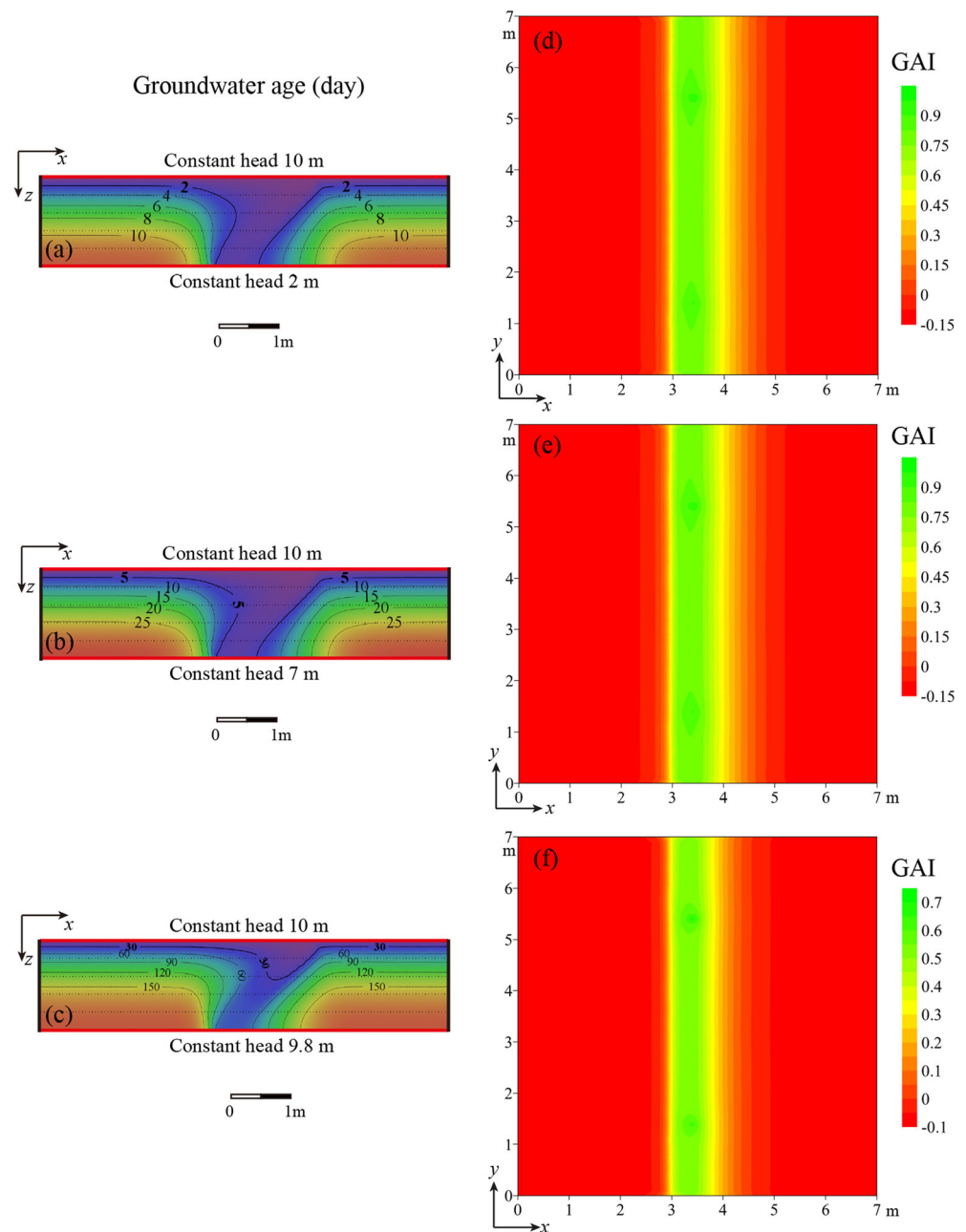
Fig. 10 **a** Plan view and **b** cross-section view of model grid and boundary conditions in the Betts Creek Beds for groundwater flow and age simulation
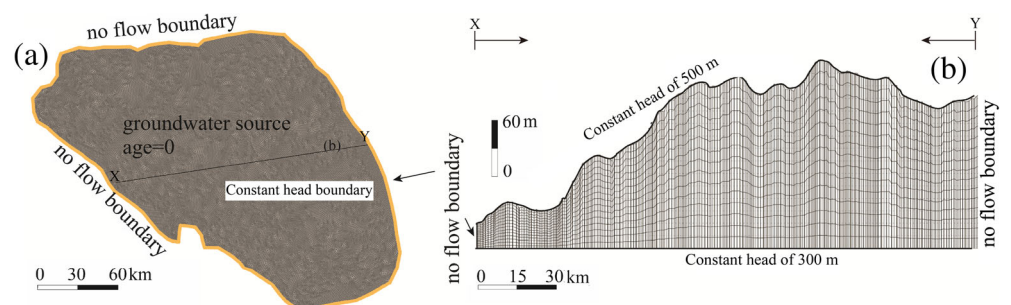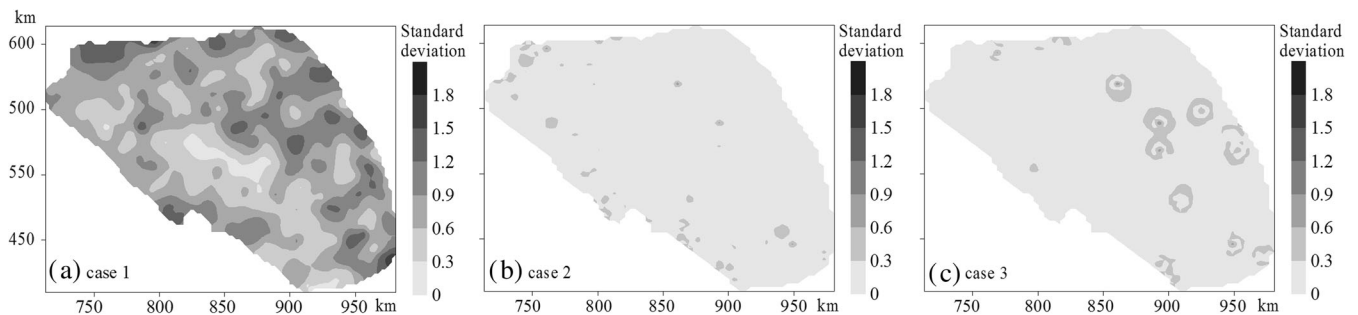
Fig. 11 The standard deviation of normalized groundwater age indicator (GAI) from ten realizations of the BCB in **a** case 1, **b** case 2 and **c** case 3

Case 1. Uncertainty in the sedimentary environment. Ten realizations of BCB are generated by SFPM and SGS. The statistics of these ten realizations are illustrated in Fig. 3, and represent the influences of the uncertainties in the quantification of the sedimentary environment that formed the BCB (including the uncertainties in the factors such as riverbed slope, sediment input, sediment input ratio and river discharge).

Case 2. Uncertainty in lithology sequence. Due to the scarcity of the lithology logs, SGS and SFPM only yield the total thickness of the sandstone and siltstone in the BCB, but the detailed sequences of sandstone and siltstone is unknown. One SGS realization (Fig. 3a,d) was arbitrarily selected and then the sandstone and siltstone were rearranged into 15 layers to generate 10 realizations of BCB with different lithology sequences. For example, at an arbitrary position of the BCB with a given thickness of 100 m, the total thickness of sandstone is 30 m and siltstone is 70 m. The sandstone is considered as 30 elements and siltstone is composed of 70 elements, with each element having a thickness of 1.0 m. A layer number from 1 to 15 is then randomly assigned to each element. As a consequence, the elements of sandstone and siltstone are redirected to different layers. The new sandstone and siltstone sequence are reconstructed, with the total thickness of sandstone and siltstone unchanged, but with different sandstone proportions in different layers.

Case 3. Uncertainty in K_s and K_c measurements. The hydraulic conductivity of sandstone (K_s) ranges from 0.01 to 0.1 m/d according to the drill stem tests. On the

basis of the lithology architecture in Fig. 3a,d, five realizations of BCB were generated by imposing K_s as 0.01, 0.03, 0.05, 0.07 and 0.09, respectively and fixing K_c as 5×10^{-7} m/d in Eqs. (1)–(3). The hydraulic conductivity of siltstone (K_c) ranges from 10^{-6} to 10^{-7} m/d according to the centrifuge permeameter tests. Another five realizations are generated by using K_c as 1×10^{-7}, 3×10^{-7}, 5×10^{-7}, 7×10^{-7}, 9×10^{-7} m/d and fixing K_s as 0.038 m/d.

The GAI is normalized in order to compare the impacts of the sedimentary environment, lithology sequence and hydraulic tests. The statistics of normalized GAI are then calculated based on ten hydraulic parameter realizations in each case. As shown in Fig. 11, the standard deviations of GAI for case 2 and case 3 are generally lower than 0.3 (Fig. 11b,c), indicating that in this work both the lithology sequences and the values of K_s and K_c have limited impacts on the estimation of the normalized GAI distribution. The uncertainty in normalized GAI distribution is mainly attributed to the uncertainty in characterizing the sedimentary environment (case 1).The spatial distribution of the normalized GAI is then inferred from ten realizations of the BCB in case 1. As a result, GAI is lower in the east and increases toward the western margin of the domain (Fig. 12a). This trend is related to the BCB thickness (Fig. 3e) as well as the groundwater flow pattern in the BCB.

The GAI distribution suggests that for gas extraction from the Aramac Coal Measure, depressurization in the east is better than in the west, as less impact will be produced on the

Fig. 12 a The mean value and **b** standard deviation of the normalized groundwater age indicator (GAI) for the BCB, suggesting the risk of connection between the underlying coalbed and the overlying aquifer
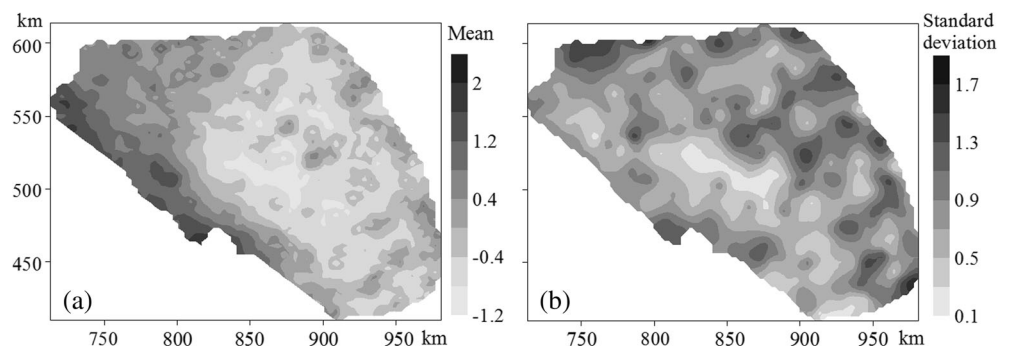
overlying aquifer via the BCB. However, it is also worth mentioning that the GAI estimation in the east presents larger uncertainties (Fig. 12b), because fewer downhole logs were obtained in this region, which leads to a larger uncertainty in quantifying the BCB heterogeneity (Fig. 1c).

Conclusion

This study proposed a GAI to quantify the degree of hydraulic connection between two water-bearing formations accounting for the large-scale heterogeneity of the separating aquitard. The GAI was determined by coupled transient groundwater flow and groundwater age simulations, which fully consider both the lateral and vertical flow processes in the aquitard and it was validated in a synthetic case by water-level responses at the aquitard top that are induced by depressurization at the aquitard bottom. These tests confirmed that depressurization locations with higher GAI can induce stronger water-level responses in the adjacent aquifer.

The GAI was then applied to estimate the hydraulic connection between the Aramac Coal Measures and the GAB via the Betts Creek Beds. The sensitivity of the GAI was examined regarding to the uncertainties in the sedimentary environment, lithology sequence and hydraulic conductivity measurements. As a consequence, the uncertainties in the sedimentary environment presented the largest impact on the GAI estimation. The statistics of GAI were then estimated, resulting in the higher GAI values in the western part of the north GB. Therefore, from an environmental impact point of view, it is safer to locate gas/water extraction wells in the east of the basin because it will lead to a lesser impact on the overlying aquifer.

Economic considerations are beyond the scope of this study; however, the approach used in this study could be combined with information on gas quality and reserves (quantity) in future studies in order to define optimal areas for CSG groundwater extraction that maximize gas production and minimize the impacts of aquifer drawdown.

References

Allen JP, Fielding CR (2007) Sedimentology and stratigraphic architecture of the Late Permian Betts Creek Beds, Queensland, Australia. Sediment Geol 202:5–34. doi:10.1016/j.sedgeo.2006.12.010

Anna LO (2003) Groundwater flow associated with coalbed gas production, Ferron Sandstone, east-central Utah. Int J Coal Geol 56:69–95. doi:10.1016/S0166-5162(03)00077-6

Beckers J, Cook T (2013) Groundwater risks associated with coal seam gas development in the Surat and southern Bowen basins. Dept. of Natural Resources and Mines, Queensland, Australia, 175 pp

Bianchi M, Zheng C, Wilson C, Tick GR, Liu G, Gorelick SM (2011) Spatial connectivity in a highly heterogeneous aquifer: from cores to preferential flow paths. Water Resour Res 47, W05524

Birkholzer JT, Zhou Q, Tsang C-F (2009) Large-scale impact of CO$_2$ storage in deep saline aquifers: a sensitivity study on pressure response in stratified systems. Int J Greenhouse Gas Control 3:181–194

Cao G, Zheng C, Scanlon BR, Liu J, Li W (2013) Use of flow modeling to assess sustainability of groundwater resources in the North China Plain. Water Resour Res 49(1):159–175

De Marsily G, Delay F, Gonçalvès J, Renard P, Teles V, Violette S (2005) Dealing with spatial heterogeneity. Hydrogeol J 13:161–183

Dell'Arciprete D, Vassena C, Baratelli F, Giudici M, Bersezio R, Felletti F (2014) Connectivity and single/dual domain transport models: tests on a point-bar/channel aquifer analogue. Hydrogeol J 22:761–778. doi:10.1007/s10040-014-1105-5

Diersch H (2002) FEFLOW: finite element subsurface flow and transport simulation system—reference manual. WASY, Berlin

Evans P (1980) Geology of the Galilee Basin. In: The geology and geophysics of northeastern Australia. Geological Society of Australia, Sydney, pp 299–305

Freeze RA, Cherry JA (1977) Groundwater. Prentice-Hall, Upper Saddle River, NJ

Frost C, Pearson B, Ogle K, Heffern E, Lyman R (2002) Sr isotope tracing of aquifer interactions in an area of accelerating coal-bed methane production, Powder River Basin, Wyoming. Geology 30:923–926

Gasda SE (2010) Numerical models for evaluating CO2 storage in deep saline aquifers: leaky wells and large-scale geological features. Princeton-Bergen Series on Carbon Storage, Princeton University, Princeton, NJ

Giambastiani BMS, McCallum AM, Andersen MS, Kelly BFJ, Acworth RI (2012) Understanding groundwater processes by representing aquifer heterogeneity in the Maules Creek Catchment, Namoi Valley (New South Wales, Australia). Hydrogeol J 20:1027–1044. doi:10.1007/s10040-012-0866-y

Habermehl M (2006) The Great Artesian basin, Australia. In: Foster S, Loucks D (2006) Non-renewable groundwater resources. UNESCO-IHP, IHPVI, Series 82, UNESCO, New York

Hamawand I, Yusaf T, Hamawand SG (2013) Coal seam gas and associated water: a review paper. Renew Sust Energ Rev 22:550–560

Harbaugh AW, Banta ER, Hill MC, McDonald MG (2000) MODFLOW-2000, the US Geological Survey modular ground-water model: user guide to modularization concepts and the ground-water flow process. US Geological Survey, Reston, VA

Hawkins P, Green P (1993) Exploration results, hydrocarbon potential and future strategies for the northern Galilee Basin. APPEA J 33:280–280

Helmuth M (2008) Scoping study: groundwater impacts of coal seam gas development—assessment and monitoring. Centre for Water in the Minerals Industry, The University of Queensland,St Lucia, Australia

Horne RN (1995) Modern well test analysis. Petroway, Palo Alto, CA

Jiang Z, Mariethoz G, Farrell T, Schrank C, Cox M (2015) Characterization of alluvial formation by stochastic modelling of paleo-fluvial processes: the concept and method. J Hydrol 524:367–377

Jiang Z, Mariethoz G, Raiber M, Timms W, Cox M (2016) Application of 1D paleo-fluvial process modelling at a basin scale to augment sparse borehole data: example of a Permian formation in the

Galilee Basin, Australia. Hydrol Process 30:1624–1636. doi:10.1002/hyp.10747

Knudby C, Carrera J (2005) On the relationship between indicators of geostatistical, flow and transport connectivity. Adv Water Resour 28:405–421

Knudby C, Carrera J (2006) On the use of apparent hydraulic diffusivity as an indicator of connectivity. J Hydrol 329:377–389. doi:10.1016/j.jhydrol.2006.02.026

Kolditz O, Ratke R, Diersch H-JG, Zielke W (1998) Coupled groundwater flow and transport: 1. verification of variable density flow and transport models. Adv Water Resour 21:27–46. doi:10.1016/S0309-1708(96)00034-6

Koltermann CE, Gorelick SM (1996) Heterogeneity in sedimentary deposits: a review of structure-imitating, process-imitating, and descriptive approaches. Water Resour Res 32:2617–2658

Michaelides K, Chappell A (2009) Connectivity as a concept for characterising hydrological behaviour. Hydrol Process 23:517–522. doi:10.1002/hyp.7214

Morin RH (2005) Hydrologic properties of coal beds in the Powder River Basin, Montana: I, geophysical log analysis. J Hydrol 308:227–241. doi:10.1016/j.jhydrol.2004.11.006

Moya CE, Raiber M, Taulis M, Cox ME (2015) Hydrochemical evolution and groundwater flow processes in the Galilee and Eromanga basins, Great Artesian Basin, Australia: a multivariate statistical approach. Sci Total Environ 508:411–426. doi:10.1016/j.scitotenv.2014.11.099

Myers T (2009) Groundwater management and coal bed methane development in the Powder River Basin of Montana. J Hydrol 368:178–193

Oriani F, Renard P (2014) Binary upscaling on complex heterogeneities: the role of geometry and connectivity. Adv Water Resour 64:47–61. doi:10.1016/j.advwatres.2013.12.003

Remy N, Boucher A, Wu J (2009) Applied geostatistics with SGeMS: a user's guide. Cambridge University Press, Cambridge, UK

Renard P, Allard D (2013) Connectivity metrics for subsurface flow and transport. Adv Water Resour 51:168–196. doi:10.1016/j.advwatres.2011.12.001

Sharma S, Frost CD (2008) Tracing coalbed natural gas-coproduced water using stable isotopes of carbon. Ground Water 46:329–334. doi:10.1111/j.1745-6584.2007.00417.x

Storey RG, Howard KW, Williams DD (2003) Factors controlling riffle-scale hyporheic exchange flows and their seasonal changes in a gaining stream: a three-dimensional groundwater flow model. Water Resour Res 39:1034

Timms W, Crane R, Anderson D, Bouzalakos S, Whelan M, McGeeney D, Rahman P, Guinea A, Acworth R (2014) Vertical hydraulic conductivity of a clayey-silt aquitard: accelerated fluid flow in a centrifuge permeameter compared with in situ conditions. Hydrol Earth Syst Sci Discuss 11:3155–3212

Winter TC (1999) Relation of streams, lakes, and wetlands to groundwater flow systems. Hydrogeol J 7:28–45

Zhang XM, Tong DK, Xue LL (2009) Numerical simulation of gas–water leakage flow in a two layered coalbed system. J Hydrodyn Ser B 21:692–698. doi:10.1016/S1001-6058(08)60201-2

Zinn B, Harvey CF (2003) When good statistical models of aquifer heterogeneity go bad: a comparison of flow, dispersion, and mass transfer in connected and multivariate Gaussian hydraulic conductivity fields. Water Resour Res 39:1051. doi:10.1029/2001wr001146